1 Materials and Experiment

1.1 Synthesis of CuHCF

All chemical reagents were purchased from Sinopharm Chemical Reagent Co., Ltd., Beijing, China, were of analytical grade, and were used without further processing or purification. First, the Prussian blue analogue (CuHCF) was synthesised using a chemical precipitation method, and 2 mmol $Cu(NO_3)_2$ with 0.5 g polyvinyl pyrrolidone (PVP, K30) was added to 1 mmol $K_3[Fe(CN)_6]$. After 12 h, the as-prepared yellow precipitate was collected via centrifugation and rinsed several times with ethanol and deionized water. Then, CuHCF was successfully obtained via vacuum drying at 60 °C.

1.2 Synthesis of CuHCF@PVA/PPy CPH

First, 3 g of polyvinyl alcohol (PVA) was dissolved in deionized water at 95 °C, stirred for several hours until a homogeneous transparent solution was formed, and then placed into an ice bath container with slight stirring. Pyrrole (0.5 mL) was then added to the PVA solution and stirred for 30 min. Then, 0.5 g of ammonium persulfate (APS) in deionized water (20 mL) was slowly dropped into the above solution, and a dark homogeneous sticky PVA/PPy solution was formed. Subsequently, 2 mmol of $Cu(NO_3)_2$ and 0.5 g of PVP were dissolved in 20 mL of deionized water and poured into the PVA/PPy solution. After adding 1 mmol of $K_3[Fe(CN)_6]$ and stirring for 30 min, the solution was subjected to five cycles of liquid nitrogen freeze-thawing, in which the mixture was frozen for 30 min and thawed for 30 min in a water bath at 40 °C. Subsequently, the hydrogel was immersed in a large amount of deionized water for 12 h. Finally, CuHCF@PVA/PPy CPH was obtained.

1.3 Electrochemical and desalination measurements

The CuHCF and carbon electrodes were fabricated with a mass ratio of active materials: poly (vinylidene fluoride) (PVDF):carbon black of 8:1:1. The CuHCF@PVA/PPy electrode was fabricated by pressing the hydrogel into a thin film at 10 Mpa for 5 min. The electrochemical performances of CuHCF and CuHCF@PVA/PPy were evaluated using cyclic voltammetry (CV), galvanostatic charge-discharge (GCD), and electrochemical impedance spectroscopy (EIS) in a 1 M NaCl electrolyte, where Pt and silver/silver chloride (Ag/AgCl) were used as the counter electrode and reference electrode, respectively. CV, GCD, and EIS measurements were performed using a CHI 600D electrochemical workstation (Shanghai CH Instruments Co., China).

The desalination performance was tested using a dual-ion device with CuHCF or CuHCF@PVA/PPy as the cathode and activated carbon as the anode. A cation exchange membrane (CEM) and anion exchange membrane (AEM) were placed in front of the CuHCF@PVA/PPy and AC electrodes, respectively. The charging and discharging processes were achieved by applying a constant potential or current, respectively. A 40 mL, 1 M NaCl solution was used as the electrolyte. The synthetic NaCl solution was continuously delivered from the beaker to the ECDI cell at a flow rate of 20 mL min^{-1}. Throughout the reaction, changes in solution conductivity and current were recorded using a conductivity meter (S230, Mettler Toledo,

Switzerland) and a power source (LAND battery testing system), respectively. Notably, the mass of a single working electrode was used to calculate the salt-adsorption capacity and rate as well as the energy consumption and recovery in the constant current mode. Moreover, the total active mass of the two electrodes was used to calculate the desalination capacity in constant-voltage mode. The desalination capacity, rate, energy consumption, and recovery were calculated using Equations (S1-S3).

1.4 Characterization

The morphologies of the obtained samples were characterized using scanning electron microscopy (S-4800, Hitachi, Japan) and transmission electron microscopy (JEM-2100F, JOEL, Japan). In addition, Belsorp-max (Microtrac BEL, Japan) was applied to estimate the specific surface area and pore structure based on the nitrogen adsorption isotherm. X-ray diffraction (XRD, D8 Advance X, Bruker, Germany) was utilized to examine the crystal structures using Cu Kα radiation (λ=0.15418 nm). X-ray photoelectron spectroscopy data was tested using a spectrometer (Axis Ultra DLD, Kratos Analytical, UK) with monochromatic Al Kα X-rays at a base pressure of 1×10^{-7} Pa. The peak energies were calibrated by placing the major C 1s peak at 284.8 eV. The water contact angles of the electrodes were calculated using dynamic contact-angle analysis (JC2000D2W, Beijing Zhongyi Kexin Technology Co., Ltd., China). Then, 3 μL of water was dropped on the surface of the electrode, and a series of images were captured as a function of contact time. The thermal stability of the samples was measured using thermogravimetry (SDTQ-600, TA instruments, USA) under air flow with a heating rate of 10 ℃·min^{-1}.

2 Computational formulas

The specific adsorption capacity (SAC, mg·g^{-1}), time-average specific adsorption rate (ASAR, mg·g^{-1}·min^{-1}), and energy consumption (ω, kWh·kg^{-1}) were calculated using Equations (S1-S3), respectively:

$$SAC=\frac{(C-C_0)V}{M} \quad \text{Eq.(S1)}$$

$$ASAR=\frac{SAC}{t}\times 60 \quad \text{Eq.(S2)}$$

$$\omega=\frac{v\times \int i\,dt}{3.6\times (C-C_0)\times V} \quad \text{Eq.(S3)}$$

where C (mg L^{-1}) and C_0 (mg L^{-1}) are the final and initial concentrations, respectively; V (L) represents the solution volume; M (g) is the mass of the electrode materials; t is charging time (s); v stands for the applied voltage (V); and i is the current (A).

The capacity (mAh·g^{-1}) investigated at various current densities was calculated as follows:

$$C=\gamma\times t, \quad \text{Eq.(S4)}$$

where γ is the current density ($mA \cdot g^{-1}$), and t is the time of the charge or discharge process (h).

The overall capacity contribution of the active materials should be a combination of sodium diffusion-controlled and capacitive processes. The relative contribution between these processes was identified based on the following power law:

$$i = av^b, \quad \text{Eq. (S5)}$$

where i is the current, v is the scan rate, and a and b are constants.

CV curves at different scan rates were used to quantify the contributions from the capacitive process (k_1v) and diffusion-controlled process ($k_2v^{1/2}$) based on the following:

$$i_{total}=i_{insertion}+i_{capacitive}=k_1v^{\frac{1}{2}}+k_2v \quad \text{Eq.(S6)}$$

$$\frac{i(V)}{v^{\frac{1}{2}}}=k_1+k_2v^{\frac{1}{2}}, \quad \text{Eq.(S7)}$$

where k_1 and k_2 represent the “diffusion controlled constant” and “capacitive constant” at a specific potential, and i (V) is the swept current from the CV plot. Then, connecting $k_1v^{1/2}$ and k_2v at different potentials provides the diffusion-controlled capacity and capacitance capacity plots, respectively.

3 Finite element simulation

The simulation of the stress and displacement of the electrode particle material after expansion was performed using the multiphysics simulation software COMSOL Multiphysics (COMSOL Inc., Sweden). The thermal and solid mechanics modules were combined to simulate this scenario. The "thermal expansion" module was used to simulate the volume expansion of the battery particles after the chemical reaction, and the "solid mechanics" module was used to simulate the mechanical information. Then, the "multiphysics coupling" module was used to couple the two modules to simulate the particle stress and strain distribution after expansion. The size of CuHCF was set to 100 nm × 100 nm with a 10 nm layer of PVDF at the periphery, whereas the thickness of the CuHCF@PVA/PPy peripheral gel was set to 40 nm. A displacement constraint was set at the periphery of the electrode material to simulate the condition of electrode-particle limitation. The expansion ratio of CuHCF was 10%, elastic modulus was 21.3 GPa, and Poisson's ratio was 0.35. The elastic modulus of the CPHs was 100 kPa, and Poisson's ratio was 0.45. For PVDF, we assumed an isotropic behaviour with an elastic modulus of 4000 MPa and Poisson's ratio of 0.3. By setting the temperature, the electrode was expanded, and the stress and displacement distributions of the electrode were simulated.

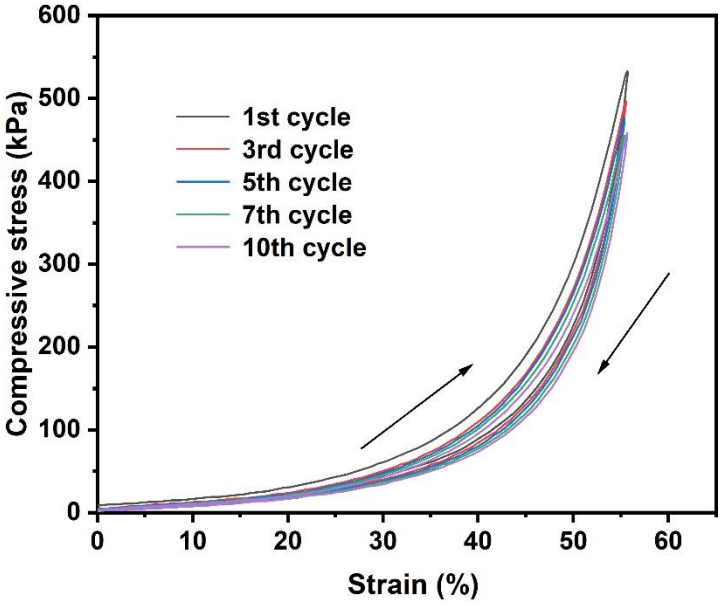

Fig. S1 Compressive stress versus strain curve of CuHCF@PVA/PPy hydrogel at 55% of maximum strain with 10 cycles.

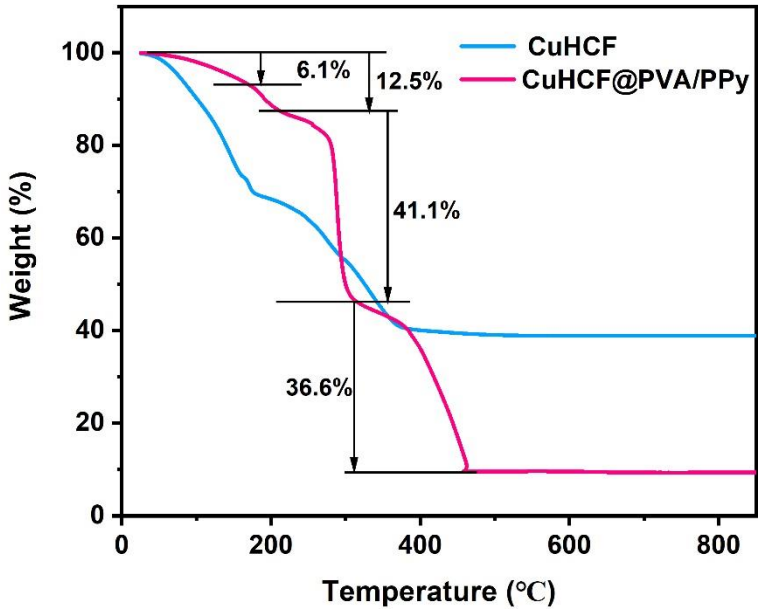

Fig. S2 TGA curves of CuHCF and CuHCF@PVA/PPy in O_2 atmosphere.

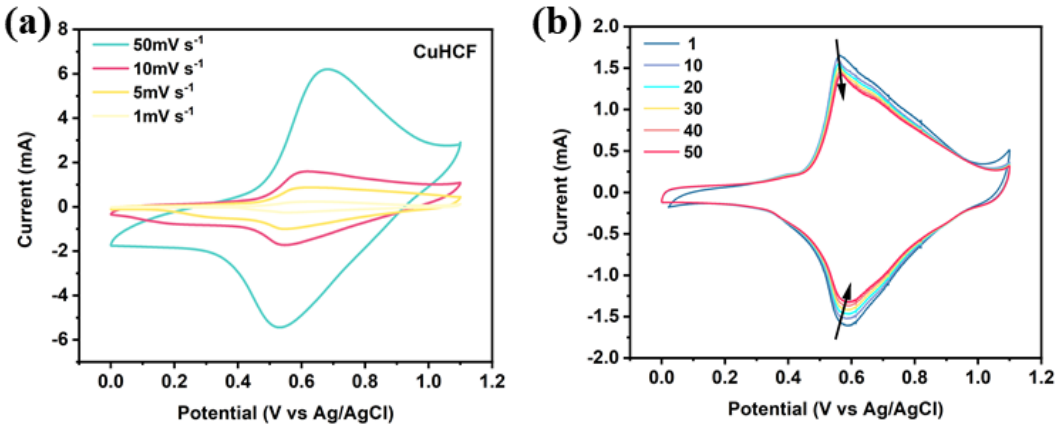

Fig. S3 (a) CV curves of CuHCF electrode in 1 M NaCl solution under different scan rates; (b) CV curves of CuHCF electrode under a scan rate of $1mV \cdot s^{-1}$ for 50 cycles.

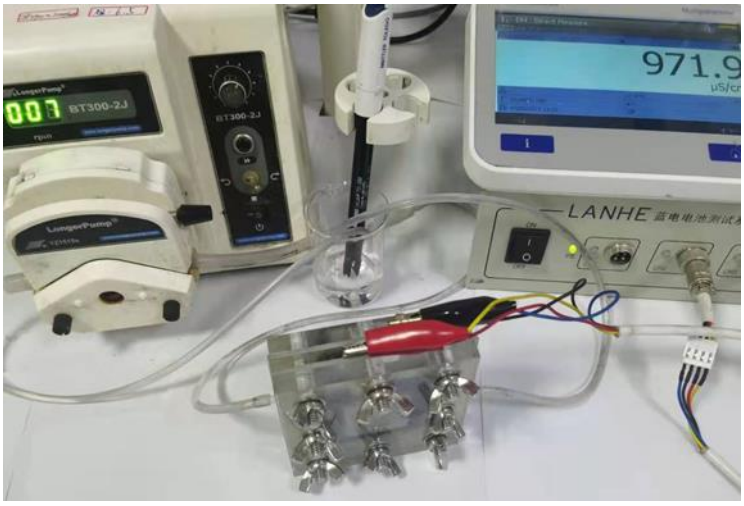

Fig. S4 Photograph of a ECDI cell.

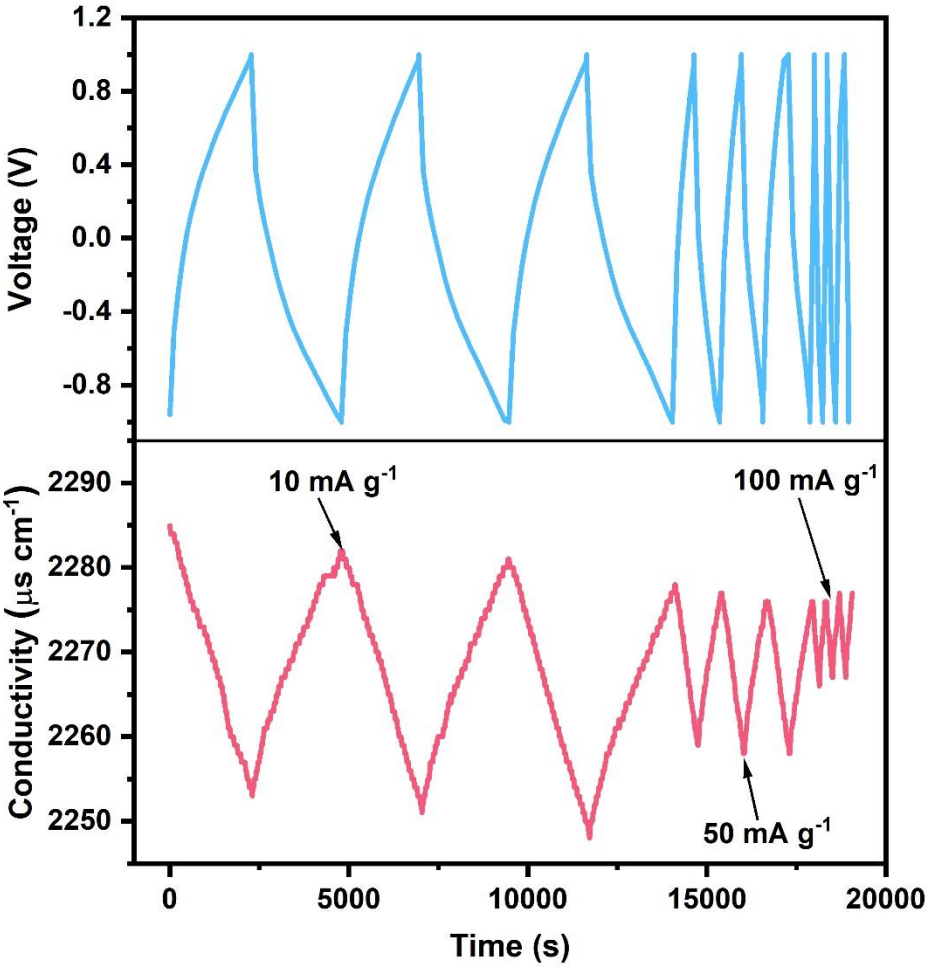

Fig. S5 The change curve of conductivity and voltage of the CuHCF@PVA/PPy with time under various current densities.

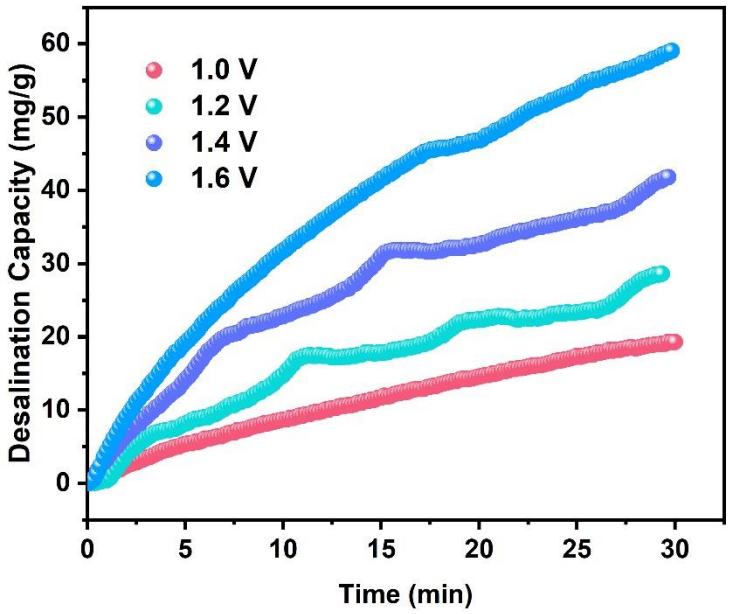

Fig. S6 Corresponding desalination capacity versus running time plots at different applied voltages.

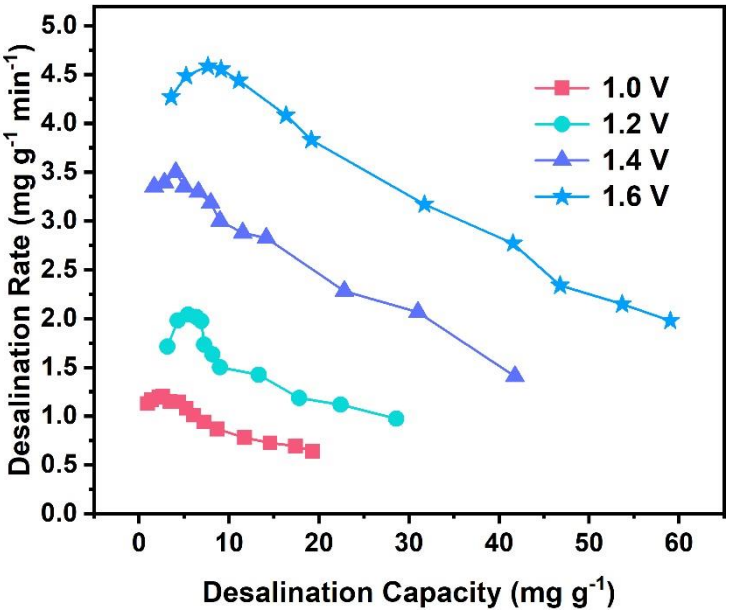

Fig. S7 Ragone plots of CuHCF@PVA/PPy with initial concentration of 1000 mg L^{-1} using different voltages.

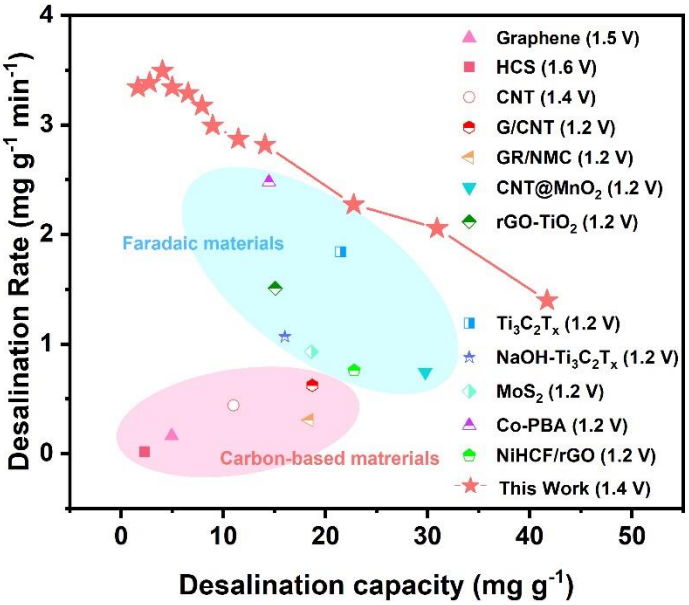

Fig. S8 Comparisons between gravimetric Ragone plots of CuHCF@PVA/PPy (Constant voltage desalination data, applied voltage: 1.4V, adsorption time: 30min) with those of other reported carbon-based and faradaic electrodes.

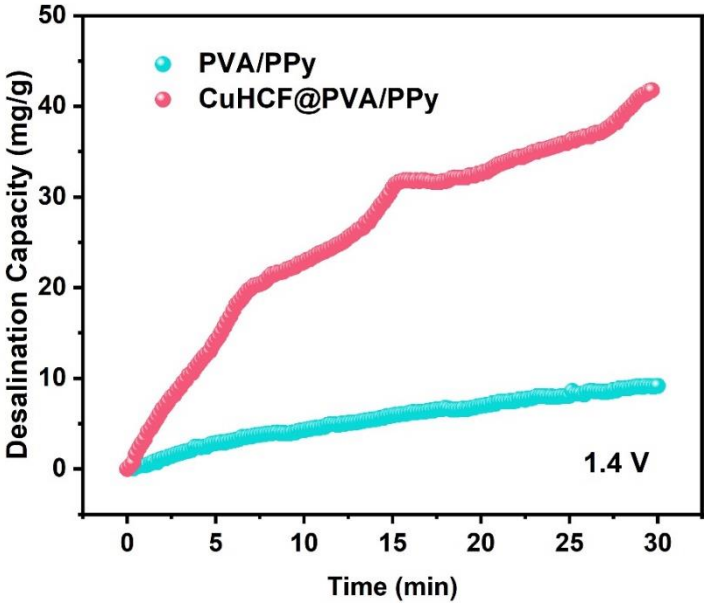

Fig. S9 Comparison of desalination capacity of CuHCF@PVA/PPy and PVA/PPy under constant voltage (1.4 V).

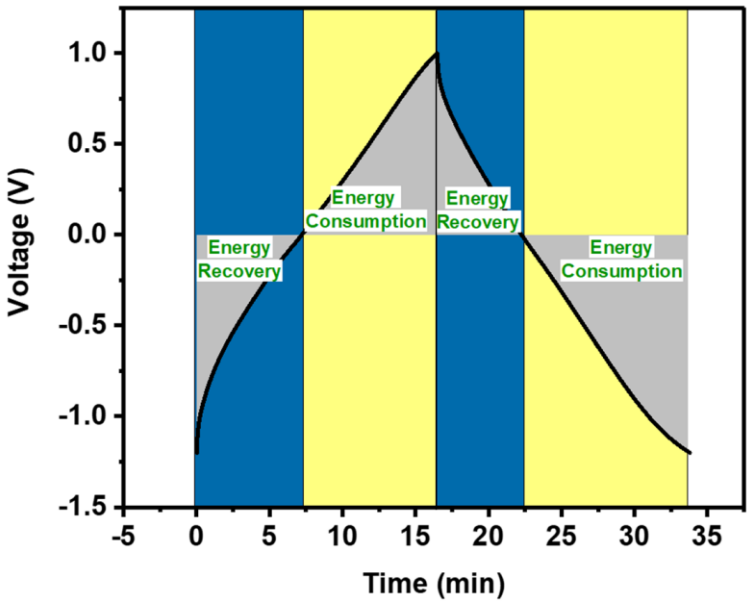

Fig. S10 Schematic of energy-consumption calculation of charging and discharging segments.

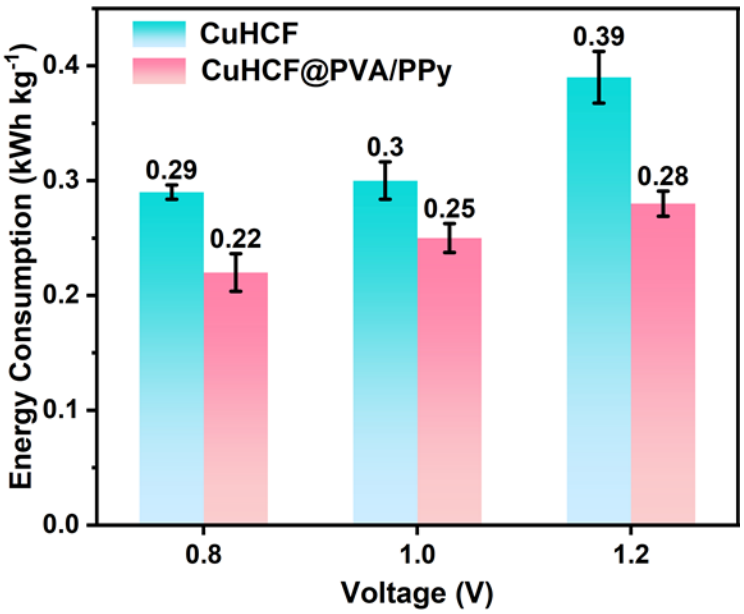

Fig. S11 Energy consumption of CuHCF and CuHCF@PVA/PPy CPH at various cut-off voltages.

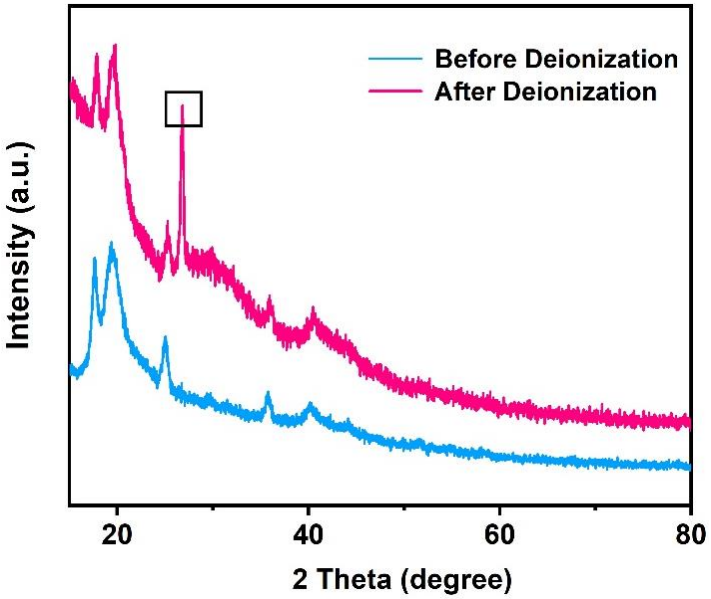

Fig. S12 XRD pattern of CuHCF@PVA/PPy before and after deionization over 100 cycles.

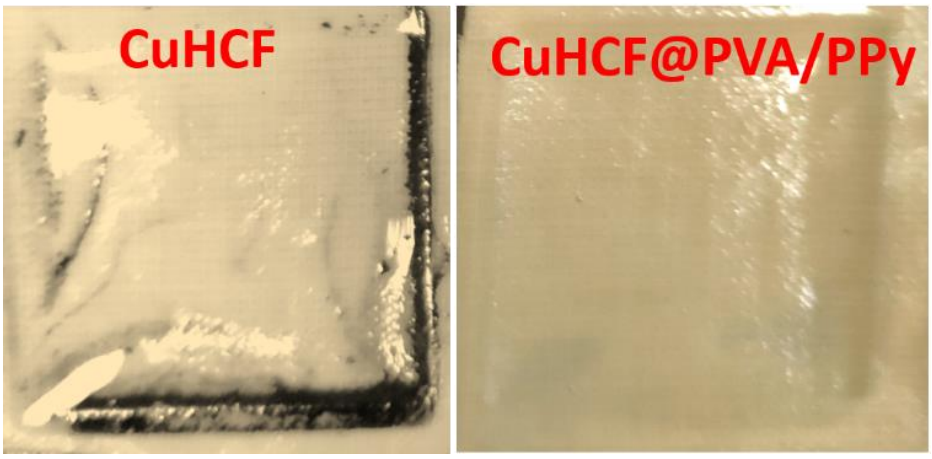

Fig. S13 Picture of CEMs of CuHCF and CuHCF@PVA/PPy electrodes after deionization for 100 cycles.

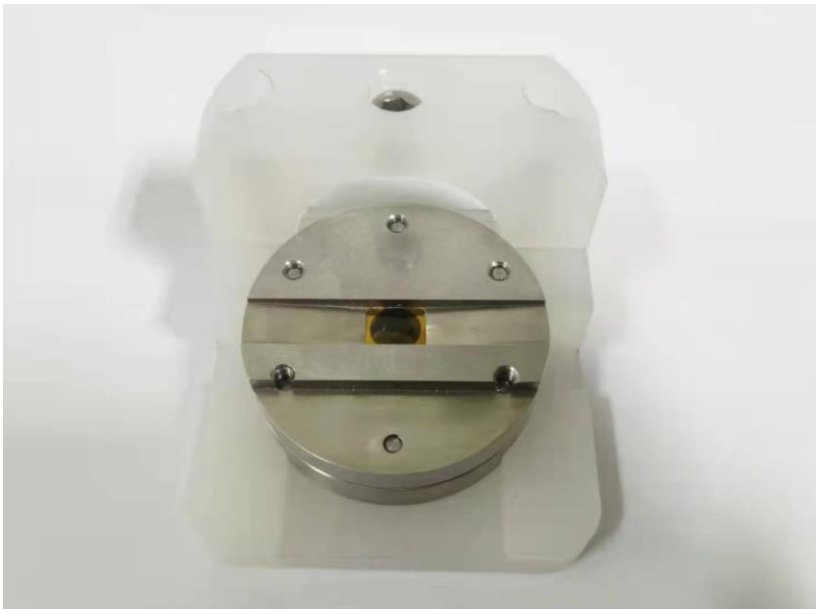

Fig. S14 In situ XRD device, including a coin-type cell, wires, and XRD holder.

Table S1. Comparison of the desalination performance of CuHCF@PVA/PPy hydrogels with those of electrodes reported in the literature.

Electrode Materials	Potential or current density	Initial Concentration (mg L^{-1})	Gravimetric desalination capacity (mg g^{-1})	Cycling stability	Ref.
Carbon Aerogel	1.2 V	260	3.3	~90% (30 cycles)	1
Graphene/CNT sponge	1.2 V	500	18.7	~100% (30 cycles)	2
N-doped GO foam	1.5 V	~ 50	4.95	99% (1000 cycles)	3
NP-EHPC	1.2 V	500	24.14	74% (150 cycles)	4
NaOH-$Ti_3C_2T_x$	1.2 V	500	16.02	95% (20 cycles)	5
MWCNT–hV_2O_5	0.8 V	35064	36.3	85% (100 cycles)	6
$Na_4Mn_9O_{18}$	1.2 V	1168.8	31.2	—	7
TiO_2-rGO	1.2 V	300	16.4	99% (25 cycles)	8
MnO_2	1.4 V	500	14.9	95.4% (350 cycles)	9
Porous Cryo-Dried MXene	1.2 V	500	27.8	~100% (60 cycles)	10

$KCuFe(CN)_6$	1.2 V	500	23.2	99.51% (100 cycles)	[11]
CuHCF/CNT	1.2 V	468	38.64	~90% (100 cycles)	[12]
Chemically Exfoliated MoS_2	1.2 V	23367	8.81	~100% (20 cycles)	[13]
NiHCF/rGO-10	1.2 V	500	22.8	78% (100 cycles)	[14]
CuHCF@PVA/PPy	10 mA g^{-1} -1.2-1.2 V	1000	45	90% (100 cycles)	This Work

Reference

1 M. Haro, G. Rasines, C. Macias and C. O. Ania, *Carbon*, 2011, **49**, 3723-3730.

2 X. Xu, Y. Liu, T. Lu, Z. Sun, D. H. C. Chua and L. Pan, *Journal of Materials Chemistry A*, 2015, **3**, 13418-13425.

3 Z.-Y. Yang, L.-J. Jin, G.-Q. Lu, Q.-Q. Xiao, Y.-X. Zhang, L. Jing, X.-X. Zhang, Y.-M. Yan and K.-N. Sun, *Advanced Functional Materials*, 2014, **24**, 3917-3925.

4 H. Zhang, C. Wang, W. Zhang, M. Zhang, J. Qi, J. Qian, X. Sun, B. Yuliarto, J. Na, T. Park, H. G. A. Gomaa, Y. V. Kaneti, J. W. Yi, Y. Yamauchi and J. Li, *Journal of Materials Chemistry A*, 2021, **9**, 12807-12817.

5 B. Chen, A. Feng, R. Deng, K. Liu, Y. Yu and L. Song, *ACS Appl. Mater. Interfaces*, 2020, **12**, 13750-13758.

6 J. Lee, P. Srimuk, K. Aristizabal, C. Kim, S. Choudhury, Y.-C. Nah, F. Mücklich and V. Presser, *ChemSusChem*, 2017, **10**, 3611-3623.

7 J. Lee, S. Kim, C. Kim and J. Yoon, *Energy & Environmental Science*, 2014, **7**, 3683-3689.

8 A. G. El-Deen, J.-H. Choi, C. S. Kim, K. A. Khalil, A. A. Almajid and N. A. M. Barakat, *Desalination*, 2015, **361**, 53-64.

9 T. Wu, G. Wang, S. Wang, F. Zhan, Y. Fu, H. Qiao and J. Qiu, *Environmental Science & Technology Letters*, 2018, **5**, 98-102.

10 W. Bao, X. Tang, X. Guo, S. Choi, C. Wang, Y. Gogotsi and G. Wang, *Joule*, 2018, **2**, 778-787.

11 S. Choi, B. Chang, S. Kim, J. Lee, J. Yoon and J. W. Choi, *Advanced Functional Materials*, 2018, **28**, 1802665.

12 Y.-H. Yang, Y.-H. Tu, H.-Y. Huang and C.-C. Hu, *Desalination*, 2023, **545**, 116160.

13 F. Xing, T. Li, J. Li, H. Zhu, N. Wang and X. Cao, *Nano Energy*, 2017, **31**, 590-595.

14 Z. Ding, X. Xu, Y. Li, K. Wang, T. Lu and L. Pan, *Desalination*, 2019, **468**, 114078.